

This manuscript has been authored by UT-Battelle, LLC, under Contract No. DE-AC05-00OR22725 with the U.S. Department of Energy. The United States Government retains and the publisher, by accepting the article for publication, acknowledges that the United States Government retains a non-exclusive, paid-up, irrevocable, world-wide license to publish or reproduce the published form of this manuscript, or allow others to do so, for the United States Government purposes. The Department of Energy will provide public access to these results of federally sponsored research in accordance with the DOE Public Access Plan (<http://energy.gov/downloads/doe-public-access-plan>).

Compressive sensing on diverse STEM scans: real-time feedback, low-dose and dynamic range

Xin Li, Ondrej Dyck, Sergei V. Kalinin* and Stephen Jesse*

The Institute of Functional Imaging Materials

And

The Center for Nanophase Materials

Oak Ridge National Laboratory, Oak Ridge, TN 37832

Abstract

Scanning Transmission Electron Microscopy (STEM) has become the main stay for materials characterization on atomic level, with applications ranging from visualization of localized and extended defects to mapping order parameter fields. In the last several years, attention was attracted by potential of STEM to explore beam induced chemical processes and especially manipulating atomic motion, enabling atom-by-atom fabrication. These applications, as well as traditional imaging of beam sensitive materials, necessitate increasing dynamic range of STEM between imaging and manipulation modes, and increasing absolute scanning/imaging speeds, that can be achieved by combining sparse sensing methods with non-rectangular scanning trajectories. Here we developed a general method for real-time reconstruction of sparsely sampled images from high-speed, non-invasive and diverse scanning pathways. This approach is demonstrated on both the synthetic data where ground truth is known and the experimental STEM data. This work lays the foundation for future tasks such as optimal design of dose efficient scanning strategies and real-time adaptive inference and control of e-beam induced atomic fabrication.

Motivation

Scanning transmission electron microscopy (STEM) has emerged as an extremely versatile imaging tool to analyze materials at atomic resolution:¹ extending from Albert Crewe's initial demonstration of single atom detection² to atomically resolved electron energy loss spectroscopy (EELS)^{3,4} and the ability of Z-contrast imaging to directly reveal structure and chemistry.⁵ The successful implementation of aberration correction not only led to record breaking resolution,^{6–9} but improved contrast and revealed the potential for 3D imaging through depth sectioning enabled by high convergence angles.^{10–13} Another impressive achievement that has been developed in recent years is the ability of EELS to access vibrational spectroscopic signals,¹⁴ adding another feather in an already impressive cap of characterization tools.

The characteristic aspect enabling the EELS modality is the energy transfer from the electron beam to a material sample, including both the electronic and ionic sub-systems.¹⁵ One manifestation of this is electron beam damage which can be brought on by direct nuclear recoil (knock-on), beam heating, radiolysis, and induced electric fields¹⁶ and is generally viewed as an effect to be avoided. Indeed, there was some question as to whether successful aberration correction would exacerbate beam damage to such an extent that it would render the advance useless.¹ Fortunately, it turned out not to be so. Nevertheless, various strategies have been employed to reduce electron dose such as repeated fast scans¹⁷ and more efficient use of the available electrons.^{18–20} It seems clear that improvements on this front will manifest in the near future where a combination of highly efficient detectors will be coupled with sparse sampling techniques for real-time, low dose imaging.

This issue has become especially acute with the recognition that the e-beam can be used for atomic scale fabrication.^{23–27} Recent efforts to manipulate single atoms with the electron beam have established that such capabilities are possible, with the introduction,²⁸ movement,^{29,30} and assembly³¹ of atoms in a graphene lattice being demonstrated. Such abilities rely on the material or atom in question to be close to being damaged by the beam. Because the same beam is used for imaging and manipulation, one must alternate between manipulation and imaging modalities in attempts to modify and then observe the sample. This requires both

increasing the dynamic range of STEM between imaging and manipulation, and increase of imaging speed, as a prerequisites to enable real-time analysis and feedback mechanisms^{32,33}. This will act to decrease the time required for observation as well as decrease the likelihood of unintentional modification of the structure being fabricated.

Recently, the approaches for sparse sensing as a pathway for low-dose STEM imaging was broadly introduced by Stevens and Browning^{21,34,35}. However, these approaches were implemented invariably for the rectangular scans of the commercial STEM systems, where the scan path is the zig-zag pattern over a rectangular area (raster scan). In other words, the electron beam is scanned from left to right, then “flies” back to the left side and scans the next row proceeding more slowly from top to bottom. A problem with this type of scan is the so-called fly-back distortion.^{36,37} This occurs due to hysteresis in the scan coils and is typically addressed by applying a delay between the fly-back step and the beginning of the next scan line which allows the scan coils to stabilize. For scanned images acquired over dozens of seconds, this delay may be an acceptably small fraction of the image acquisition time. However, because this delay is the same no matter how quickly the image is acquired, it may pose a significant lower bound on the speed with which acquisition can occur. The alternative scan paths introduced recently offer an improvement for scanning speed.³⁸ However, the dynamic range problem until recently remained unresolved.

Here, we introduce a general method for real-time reconstruction of sparsely sampled images from high-speed, non-invasive and diverse scanning pathways. A critical requirement for the practical application of such a method, assuming reliable reconstruction is given, is that it must be fast enough to operate in real time (magnitudes faster than scanning duration). To ensure its applicability in this regard, it is deployed via an NVIDIA Titan X Pascal graphics processing unit (GPU) to evaluate its performance in a favorable yet realistic context (i.e. having the computational muscle of a supercomputing cluster is certainly possible but employing a local GPU-accelerated process is much more accessible and likely). The source code used for the investigations described has been made available at [here](#). This approach is demonstrated on synthetic data and implemented on the operating STEM.

Real-time Image Inpainting

We want to recover the (unknown) full STEM image, f_0 , from sparse and noisy measurements y that can be obtained from various scanning pathways including spiral scan, raster scan, random scan and Lissajous scan that are demonstrated numerically and experimentally in following sections. Besides the noisy measurements, another input is the sampling mask, which is the spatial locations from which we have acquired the measurements, and it can be precomputed given scanning pathway and output image size. We express this in mathematical terms as,

$$y = \Phi f_0 + \epsilon \quad (1)$$

where ϵ is the measurement noise and Φ is the masking operator, defined by

$$(\Phi y)_p \stackrel{\text{def}}{=} \begin{cases} y_p & \text{if } p \in M \\ 0 & \text{otherwise} \end{cases} \quad (2)$$

where M is a binary mask indicating pixel locations sampled by scanning pathways.

We focus on using structural sparsity regularization on the redundant wavelet frame³⁹ to recover an image from the sparse measurements. The reconstructed STEM image $f = Wx$ is estimated by optimizing the coefficients x in the wavelet basis, where W is the wavelet synthesis operator. To achieve this, we solve the L_1 sparsity regularized image inpainting problem via the iterative thresholding algorithm:⁴⁰

$$\text{argmin}_x = \frac{1}{2} \|y - \Phi Wx\|^2 + \lambda \|x\|_1 \quad (3)$$

where λ is the tuning parameter controlling the sparsity. The soft thresholding operator plays a key role in the L_1 minimization that shrinks the value of coefficients:

$$S_\lambda(x) = x * \max(0, 1 - \frac{\lambda}{|x|}) \quad (4)$$

We denote the soft thresholding operator in wavelet basis as:

$$S_\lambda^W(f) = \sum_m S_\lambda(\langle f, w_m \rangle) w_m \quad (5)$$

where w_m is the basis of the wavelet frame $W = \{w_m\}$. Specifically, we focus on the Daubechies wavelets⁴¹, a family of orthogonal wavelets.

Following derivations in the iterative thresholding algorithm,^{40,42} each iteration computes:

$$f^{(i+1)} = S_\lambda^W(\text{ProjC}(f^{(i)})) \quad (6)$$

where $\text{ProjC}(f)$ computes the gradient descent of the data fidelity term $\frac{1}{2} \|y - \Phi Wx\|^2$:

$$\text{ProjC}(f) = My + (1 - M)f \quad (7)$$

To get real-time image inpainting from sparse scan measurements that is instrumental for future tasks such as real-time in-situ atom motion tracking, we developed a parallel implementation for the above iterative thresholding algorithm utilizing the CUDA toolkit of the NVIDIA Corporation. The wavelet transform is based on the PDWT⁴³ package. It costs around 0.008 seconds to reconstruct an experimental STEM image of size 256 by 256.

Sparse Spiral Scan

Although the real-time image inpainting algorithm is adapted to various scanning pathways as demonstrated in later sections, we begin by consideration of the special shape of an Archimedean spiral that avoids abrupt changes in scanning direction and has less requirements on beam control hardware, making it an efficient and hardware-friendly scanning strategy practically. Additional discussion regarding spiral scans and the associated advantages over raster scans can be found at Sang *et. al.*³⁶ One can directly control the total scanning *duration* as well as electron distribution *sparseness* via Archimedean spiral scan whose scanning pathway is determined by Eq. (7):

$$x = AT \cos(\omega T), y = AT \sin(\omega T) \quad (7)$$

Given the fixed hardware data *IO_rate*, the sampling time sequence *T* is determined by the total scanning duration, $T=[0, \text{duration}]$ with a step size of $1/\text{IO_rate}$. In practice, we normalize the *T* to $[0,1]$ with the step size of $1/(\text{IO_rate} * \text{duration})$. In this way, one can control the physical scanning area directly by the *amplitude* parameter, *A*. Taking the derivative of Eq. (7), at a particular sampling time point, *t*, we get the scanning beam velocity with a magnitude:

$$|\vec{v}| = A\sqrt{1 + \omega^2 t^2} \approx A\omega t \quad (8)$$

and the magnitude of angular velocity is defined by:

$$\Omega = \frac{|\vec{v}|}{r} = \frac{A\omega t}{t} = A\omega \quad (9)$$

As the sampling time t increases, the spiral is drawn outward beginning at the origin with the increasing velocity magnitude. This means that the center of the spiral will be more densely sampled than the outer edge. Meanwhile, given the total scanning duration, smaller frequency ω (angular velocity) will result in a shorter total scan distance, yielding spatial sparseness of electron dose distribution, and will increase the average sampling density (this will improve the signal-to-noise ratio in practice), improving evenness of electron dose distribution. Figure 1 clearly highlight sparseness and evenness introduced by decreasing frequency ω , where we scatter points on an Archimedean spiral with $\omega = 128, 16$, and 8 (Hz).

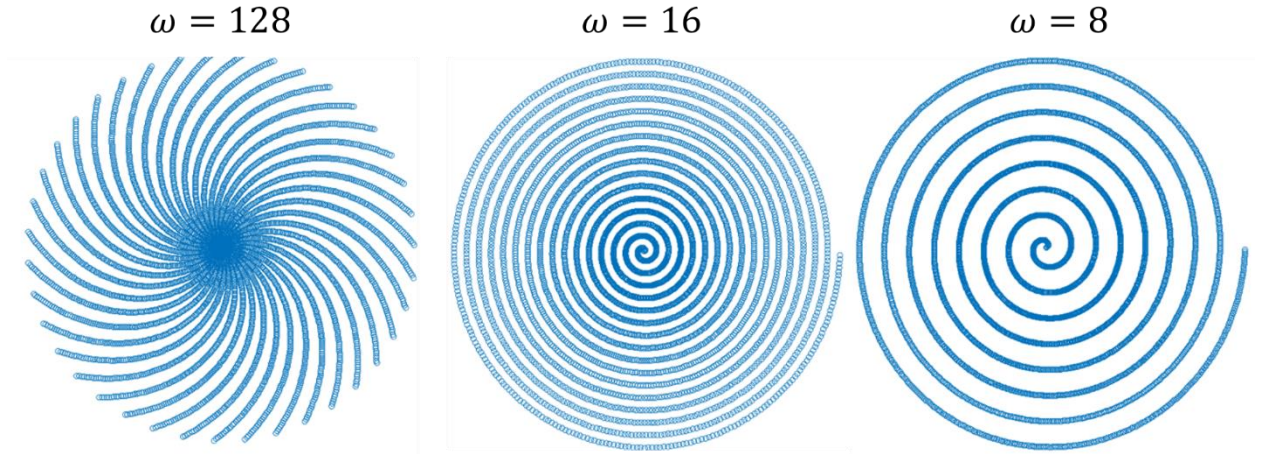


Figure 1: Dose distribution sparseness and evenness induced by small ω on Archimedean spiral scan trajectory with IO_rate = 200000 Hz, total scanning duration = 0.05 seconds and $A = 1$ v.

Results

The real-time inpainting algorithm only requires the sparse and noisy measurements y together with the sampling mask M that can be precomputed offline. To ascertain the performance of the algorithm, we first performed reconstructions with artificially sampled datasets with Archimedean scan. We use the structural similarity index (SSIM⁴⁴) for measuring inpainting quality. SSIM returns value of 1 for synthetic ground-truth image compared with itself. All experiments were performed on square images of width $N = 256$.

Synthetic Spiral Scan

Figure 2a is the synthetic ground-truth STEM image for graphene with a single 4-fold silicon dopant without any noise, whose pixel intensities was normalized to [0,1]. We added white Gaussian noise with variance $\delta^2 = 0.80$ to the Archimedean spiral scan path imposed on the ground-truth image. For Archimedean spiral, we set frequency $\omega = 8, 16, 32, 64, 128$ (Hz) with different scanning durations: 0.1, 0.2, 0.4, 0.8, 1.6 (seconds). We fixed IO_rate at 2000000 Hz and the amplitude A at 1(v). Figure 2b are the sparse and noisy images sampled by Archimedean spiral scans on the ground-truth image. In Figure 2b, we can see the outer region has more noise although the noise variance is fixed along the Archimedean spiral scans. This is because scanning beam moves faster at outer edges, yielding less samples within per pixel location. Figure 2c shows the impressive reconstruction images based on sparse and noisy ones in Figure 2b.

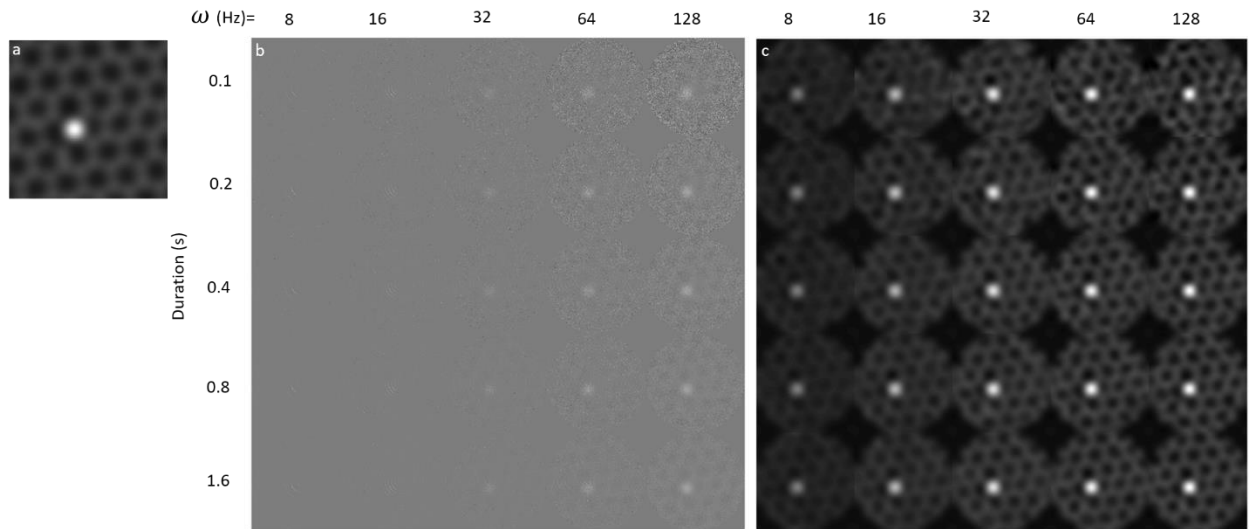


Figure 2: Synthetic Spiral Scan. (a) Ground-truth image. **(b)** Sparse and noisy Archimedean spiral scans over the ground-truth image. **(c)** Reconstructed images.

Figure 3 displays the SSIM values for all sparse and noisy measurements and the corresponding reconstruction results. Interestingly, at shortest scanning duration of 0.1 seconds, reconstruction yielded higher SSIM values with smaller frequency for $\omega = 32, 64, 128$ (Hz). This may be caused

by higher average sampling density resulted from smaller frequency as illustrated before in Figure 1.

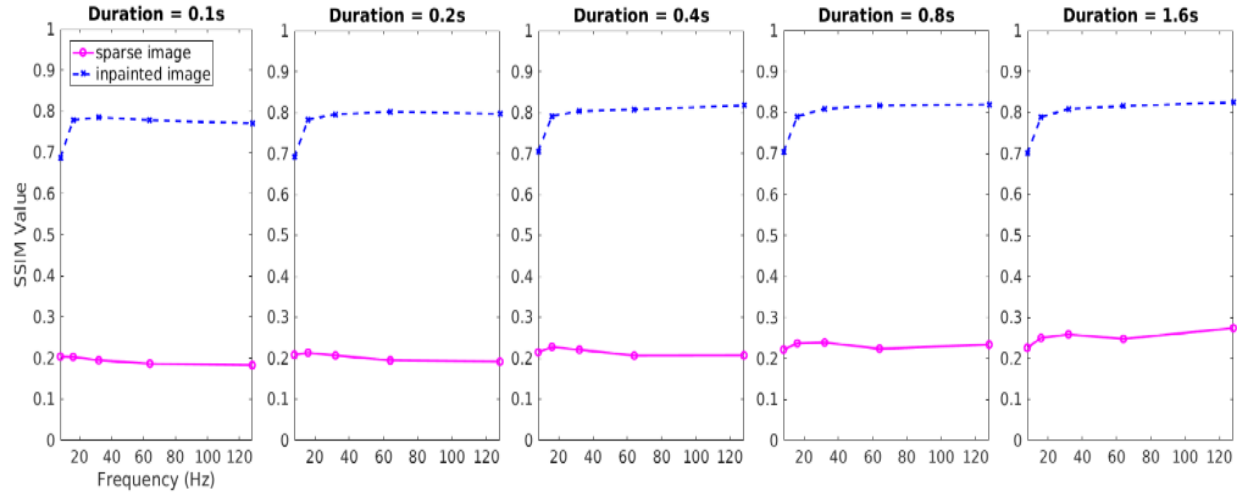


Figure 3: SSIM values of reconstruction from sparse spiral scans on simulation datasets.

Experimental Spiral Scan

We first set the amplitude of Archimedean spiral scan at $A = 5$ (v), with $\omega = 16, 32, 64, 128$ (Hz) and durations of 0.1, 0.2, 0.4, 0.8, 1.6, 3.2 (seconds). Figure 4a displays the raw STEM images by Archimedean spiral scans and Figure 4b shows the corresponding inpainted results. Figure 4c is the large view of raw Archimedean spiral scanned image with maxim duration of 6.4 seconds and maxim frequency considered at $\omega = 256$ Hz. Figure 4d,e are the large views of raw and inpainted images from Archimedean spiral scan with duration of 3.2 seconds and $\omega = 32$ Hz. At amplitude voltage of 5 (v), we see the reconstruction could not yield recognizable lattice structure with ω less than 16Hz. Also, for scans finished less than 0.8 seconds, both raw and inpainted images were severely affected by noise, making it hard to see the atomic structure.

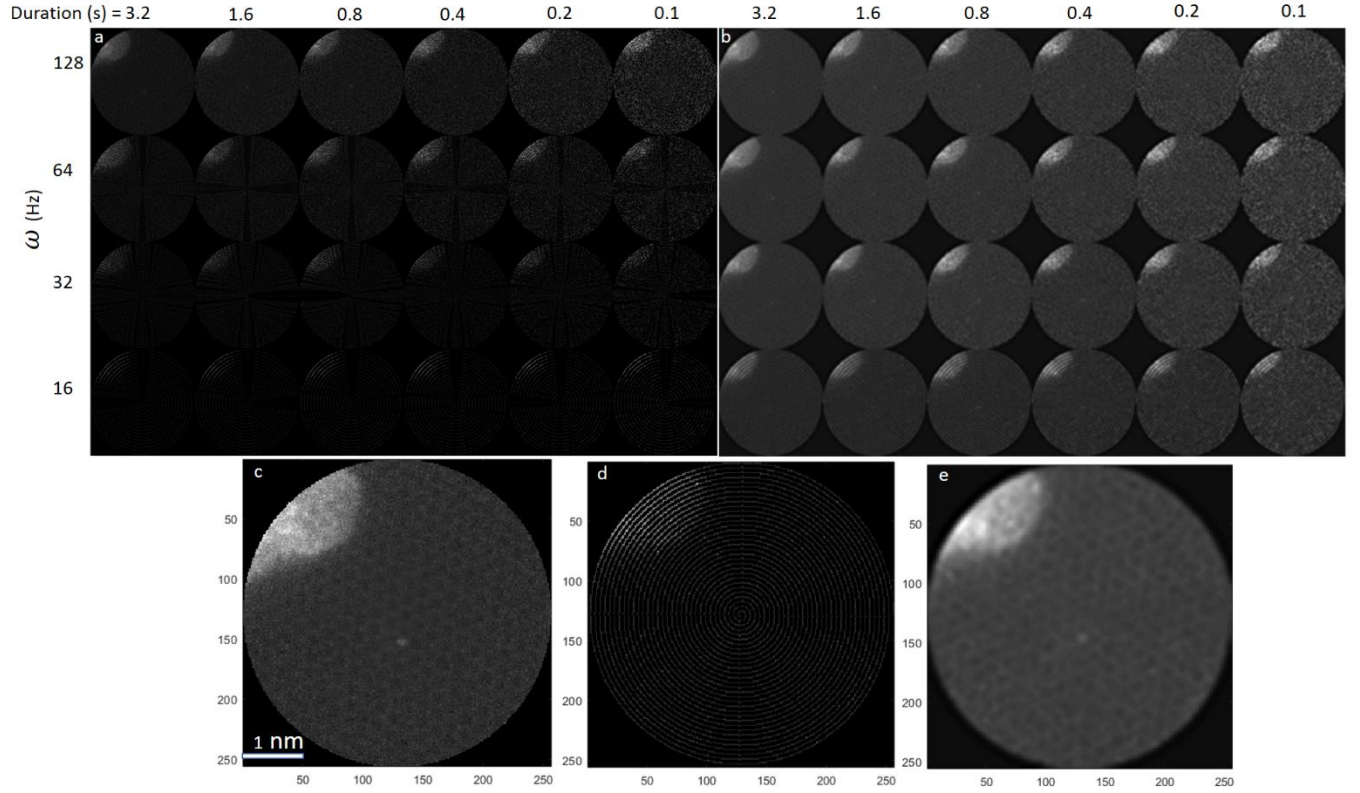


Figure 4: Experimental Archimedean spiral scans with voltage of $A = 5$ (v). (a,b) Raw and Inpainted images. (c) Raw STEM image from Archimedean spiral scan with duration of 6.4 seconds and frequency of 256 Hz. (d,e) Large views of raw and inpainted images from Archimedean spiral scan with duration of 3.2 seconds and frequency of 32 Hz.

To increase temporal resolution as well as spatial sparseness, we can straightforwardly decrease physical scanning area by reducing the amplitude of Archimedean spiral scan to $A = 1$ (v). For this smaller scanning area, we considered $\omega = 8, 16, 32, 64, 128$ Hz and durations of 0.1, 0.2, 0.4, 0.8, 1.6 seconds. Figure 5a displays raw STEM images by Archimedean spiral scans and Figure 5b shows the corresponding inpainted results. Figure 5c,d are the large views of raw and inpainted images from Archimedean spiral scan with duration of 0.8 seconds and $\omega = 32$ Hz. We note that it only took 0.8 seconds to sparsely scan over 2.5 nm^2 area, meanwhile reliable reconstruction took around 0.008 seconds.

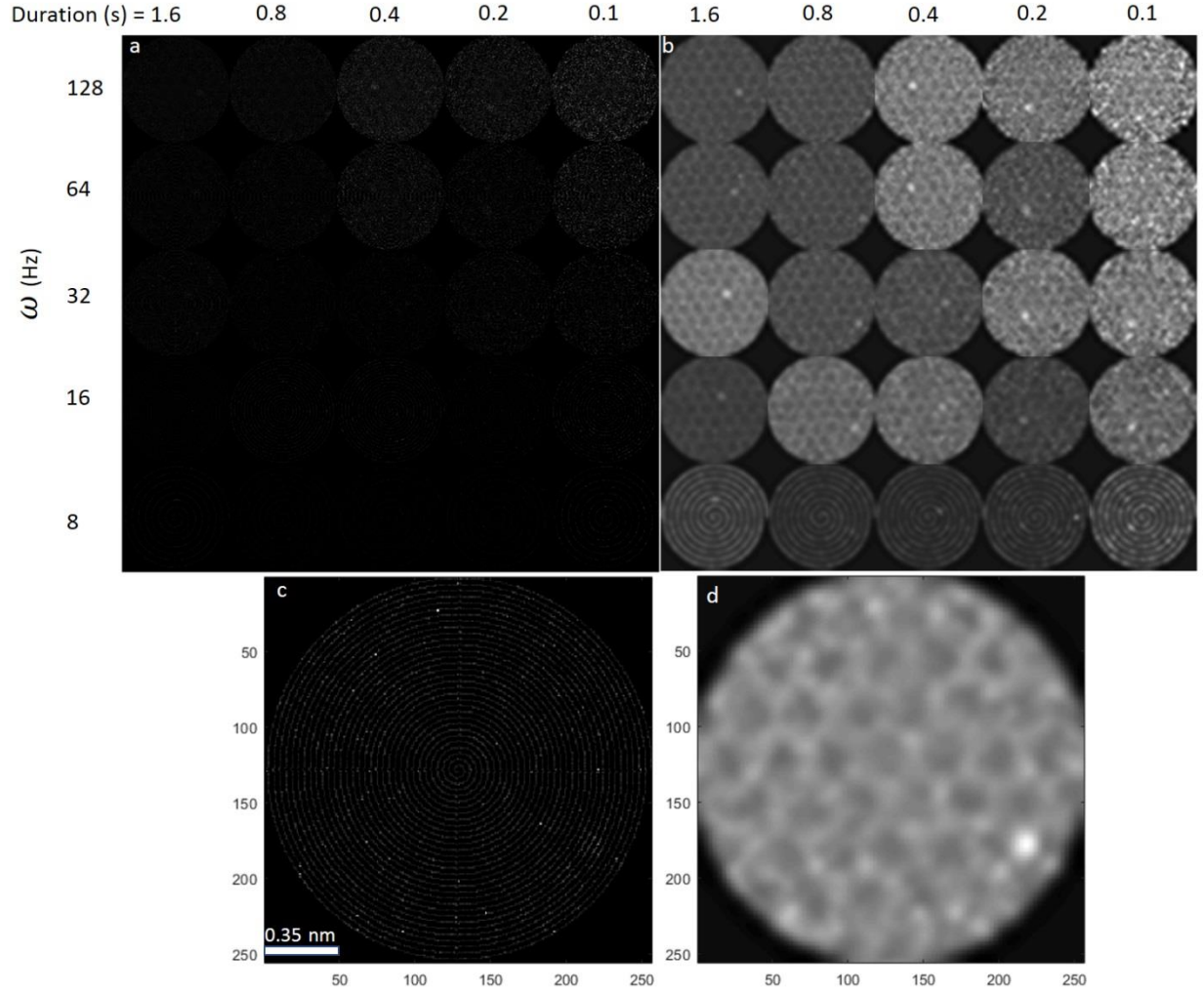


Figure 5: Experimental Archimedean spiral scans with voltage of $A=1$ (v). (a,b) Raw and Inpainted images. **(c,d)** Large views of raw and inpainted images from Archimedean spiral scan with duration of 0.8 seconds and frequency of 32 Hz.

Diverse Scanning Pathways

We first considered the random scans on the synthetic ground-truth image. Define the scanning ratio, sr , as the number of scanned pixels over the number of total pixels. We added the white Gaussian noises with $\delta^2 = 0.02, 0.05, 0.10$ and we set $sr = 0.1, 0.2, 0.3, 0.4, 0.5, 0.6, 0.7, 0.8, 0.9$. Supplementary Figure 1a displays the sparse measurements with $sr = 0.9, 0.3, 0.1$ under various noise levels. Supplementary Figure 1b are the reconstructed images and Supplementary Figure 1c are the SSIM values.

We also considered the Lissajous scans on the synthetic ground-truth image. The scan trajectory of Lissajous scan is defined as:

$$x = \cos(mT), y = \sin(nT) \quad (10)$$

We set the scanning duration to be 2π seconds. We added white Gaussian noise with variance $\delta^2 = 0.02$ to the scan path. We considered 3 combinations of (m,n) as illustrated in Supplementary Figure2.

Finally, Supplementary Figure3 shows conducted experimental raster scans and inpainting results. For experimental raster scans, we apply a constant voltage on one scanning direction while another direction is driven by a sine wave. We set duration to be 1.6 seconds with $\omega = 128, 64, 32, 16, 8$ (Hz).

Discussion

In the foreseeable future, the very same e-beam is used for both imaging mode and fabrication mode. With little hardware updates and cost, our work significantly increases the imaging temporal resolution, enabling the real-time imaging feedback mechanism, which plays a crucial rule in e-beam atom-by-atom fabrication with potential applications on manufacturing of quantum devices such as graphene qubits.⁴⁵ One immediate follow-up is incorporating current setting into live data stream analysis from microscope to perform imagining-driven, adaptive inference of e-beam induced dynamical systems, utilizing recently developed statistical learning approaches. Another uptake for the STEM community is that our work opens the pathway for the comprehensive investigation and optimal design on dose efficient scanning strategies. To further stimulate the progress for STEM community, we open-source the code online.

Materials and Methods

We design a field-programmable gate array (FPGA)-based scan system (built upon a National Instruments PXIe-1073 chassis) capable of interfacing with various microscopes. A LabView routine is developed to generate voltage waveforms with input coordinates from customized Matlab code, enabling arbitrary and dynamic beam positioning.

Inpainting algorithm has three primary tuning parameters: total iteration number, thresholding value and the level of wavelet. For all the synthetic and experimental datasets, we fixed total iteration number at 10, the thresholding value at 2.4. For scans with amplitude A of 5 (v), we choose the wavelet level to be 2. For less scanning area with the smaller amplitude A of 1 (v), we set the level to be 3, since the atom spans more pixels than those scanned at A = 5 (v). The source code can be found at [this address](#).

Acknowledgements

We gratefully acknowledge the support of NVIDIA Corporation with the donation of the Titan X Pascal GPU used for this research.

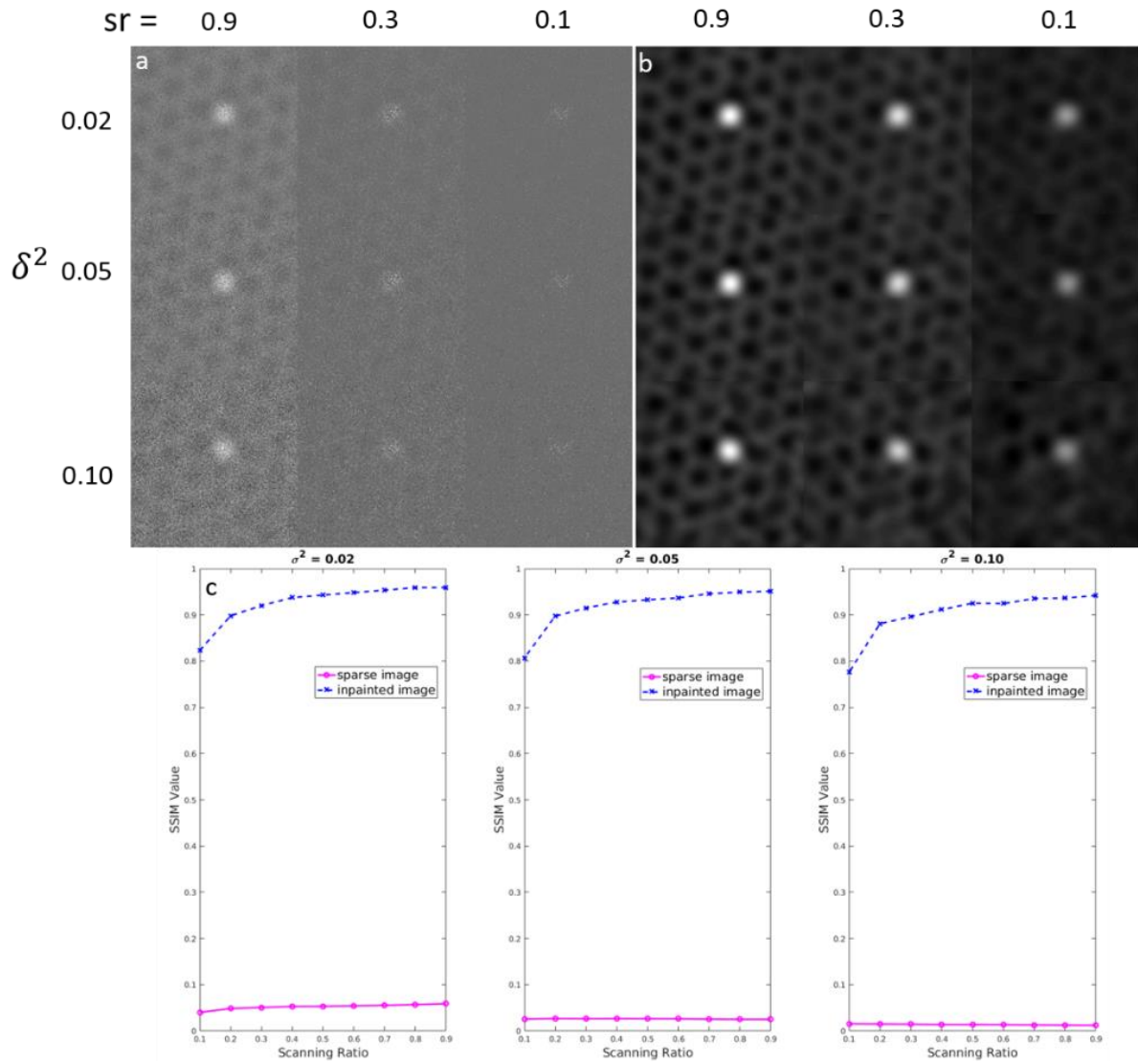
References

1. Pennycook, S. J. The impact of STEM aberration correction on materials science. *Ultramicroscopy* **180**, 22–33 (2017).
2. Crewe, A. V, Wall, J. & Langmore, J. Visibility of single atoms. *Science* **168**, 1338–40 (1970).
3. Browning, N. D., Chisholm, M. F. & Pennycook, S. J. Atomic-resolution chemical analysis using a scanning transmission electron microscope. *Nature* **366**, 143–146 (1993).
4. Batson, P. E. Simultaneous STEM imaging and electron energy-loss spectroscopy with atomic-column sensitivity. *Nature* **366**, 727–728 (1993).
5. Krivanek, O. L. *et al.* Atom-by-atom structural and chemical analysis by annular dark-field electron microscopy. *Nature* **464**, 571–574 (2010).
6. H. Rose. PHASE CONTRAST IN SCANNING TRANSMISSION ELECTRON MICROSCOPY. *Optik (Stuttg)*. **39**, 416–436 (1974).
7. Findlay, S. D. *et al.* Robust atomic resolution imaging of light elements using scanning transmission electron microscopy. *Appl. Phys. Lett.* **95**, 191913 (2009).
8. Okunishi, E. *et al.* Visualization of Light Elements at Ultrahigh Resolution by STEM Annular Bright Field Microscopy. *Microsc. Microanal.* **15**, 164–165 (2009).
9. Findlay, S. D. *et al.* Dynamics of annular bright field imaging in scanning transmission electron microscopy. *Ultramicroscopy* **110**, 903–23 (2010).
10. Borisevich, A. Y., Lupini, A. R. & Pennycook, S. J. Depth sectioning with the aberration-corrected scanning transmission electron microscope. *Proc. Natl. Acad. Sci. U. S. A.* **103**, 3044–8 (2006).
11. Borisevich, A. Y. & Y., A. Depth sectioning of aligned crystals with the aberration-corrected scanning transmission electron microscope. *J. Electron Microsc. (Tokyo)*. **55**, 7–12 (2006).
12. van Benthem, K. *et al.* Three-dimensional imaging of individual hafnium atoms inside a semiconductor device. *Appl. Phys. Lett.* **87**, 034104 (2005).
13. van Benthem, K. *et al.* Three-dimensional ADF imaging of individual atoms by through-focal series scanning transmission electron microscopy. *Ultramicroscopy* **106**, 1062–1068 (2006).
14. Krivanek, O. L. *et al.* Vibrational spectroscopy in the electron microscope. *Nature* **514**, 209–212 (2014).
15. Egerton, R. F. *Electron Energy-Loss Spectroscopy in the Electron Microscope. Book* (2011). doi:10.1007/978-1-4419-9583-4
16. Jiang, N. Electron beam damage in oxides: a review. *Reports Prog. Phys.* **79**, 016501 (2016).
17. Zhou, W. *et al.* Single Atom Microscopy. *Microsc. Microanal.* **18**, 1342–1354 (2012).
18. Pennycook, T. J. *et al.* Efficient phase contrast imaging in STEM using a pixelated detector. Part 1: Experimental demonstration at atomic resolution. *Ultramicroscopy* **151**, 160–167 (2015).
19. McMullan, G., Clark, A. T., Turchetta, R. & Faruqi, A. R. Enhanced imaging in low dose electron microscopy using electron counting. *Ultramicroscopy* **109**, 1411–1416 (2009).

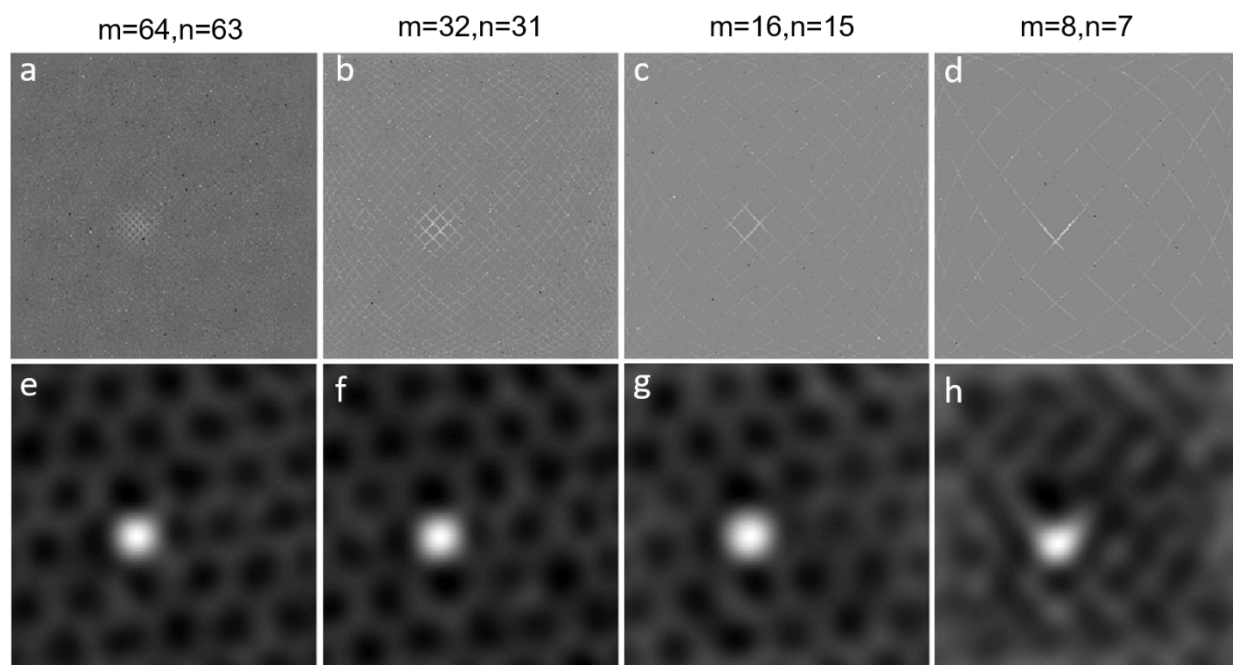
20. McMullan, G., Faruqi, A. R., Clare, D. & Henderson, R. Comparison of optimal performance at 300keV of three direct electron detectors for use in low dose electron microscopy. *Ultramicroscopy* **147**, 156–163 (2014).
21. Stevens, A., Yang, H., Carin, L., Arslan, I. & Browning, N. D. The potential for Bayesian compressive sensing to significantly reduce electron dose in high-resolution STEM images. *Microscopy* **63**, 41–51 (2014).
22. Kovarik, L., Stevens, A., Liyu, A. & Browning, N. D. Implementing an accurate and rapid sparse sampling approach for low-dose atomic resolution STEM imaging. *Appl. Phys. Lett.* **109**, (2016).
23. Kalinin, S. V., Borisevich, A. & Jesse, S. Fire up the atom forge. *Nature* **539**, 485–487 (2016).
24. Zhao, X. *et al.* Engineering and modifying two-dimensional materials by electron beams. *MRS Bull.* **42**, 667–676 (2017).
25. Kalinin, S. V. & Pennycook, S. J. Single-atom fabrication with electron and ion beams: From surfaces and two-dimensional materials toward three-dimensional atom-by-atom assembly. *MRS Bull.* **42**, 637–643 (2017).
26. Jiang, N. *et al.* Atom-by-atom fabrication by electron beam via induced phase transformations. *MRS Bull.* **42**, 653–659 (2017).
27. Susi, T. *et al.* Silicon–Carbon Bond Inversions Driven by 60-keV Electrons in Graphene. *Phys. Rev. Lett.* **113**, 115501 (2014).
28. Dyck, O., Kim, S., Kalinin, S. V. & Jesse, S. Placing single atoms in graphene with a scanning transmission electron microscope. *Appl. Phys. Lett.* (2017). doi:10.1063/1.4998599
29. Susi, T., Meyer, J. C. & Kotakoski, J. Manipulating low-dimensional materials down to the level of single atoms with electron irradiation. *Ultramicroscopy* **180**, 163–172 (2017).
30. Susi, T. *et al.* Towards atomically precise manipulation of 2D nanostructures in the electron microscope. *2D Mater.* **4**, 042004 (2017).
31. Dyck, O., Kim, S., Jimenez-Izal, E., ... A. A. preprint arXiv & 2017, undefined. Assembling Di- and Multiatomic Si Clusters in Graphene via Electron Beam Manipulation. *arxiv.org*
32. Jesse, S. *et al.* Atomic-Level Sculpting of Crystalline Oxides: Toward Bulk Nanofabrication with Single Atomic Plane Precision. *Small* **11**, 5895–5900 (2015).
33. Jesse, S. *et al.* Direct atomic fabrication and dopant positioning in Si using electron beams with active real-time image-based feedback. *Nanotechnology* **29**, 255303 (2018).
34. Kovarik, L., Stevens, A., Liyu, A. & Browning, N. D. Implementing an accurate and rapid sparse sampling approach for low-dose atomic resolution STEM imaging. *Appl. Phys. Lett.* **109**, 164102 (2016).
35. Stevens, A. *et al.* A sub-sampled approach to extremely low-dose STEM. *Appl. Phys. Lett.* **112**, 043104 (2018).
36. Muller, A. & Grazul, J. Optimizing the environment for sub-0.2 nm scanning transmission electron microscopy. *J. Electron Microsc. (Tokyo)*. (2001).
37. Jones, L. & Nellist, P. D. Identifying and correcting scan noise and drift in the scanning

- transmission electron microscope. in *Microscopy and Microanalysis* (2013).
doi:10.1017/S1431927613001402
38. Sang, X. *et al.* Dynamic scan control in STEM: spiral scans. *Adv. Struct. Chem. Imaging* **2**, 6 (2017).
 39. Mallat, S. *A Wavelet Tour of Signal Processing. A Wavelet Tour of Signal Processing* (2009).
doi:10.1016/B978-0-12-374370-1.X0001-8
 40. Daubechies, I., Defrise, M. & De Mol, C. An iterative thresholding algorithm for linear inverse problems with a sparsity constraint. *Commun. Pure Appl. Math.* (2004). doi:10.1002/cpa.20042
 41. Daubechies, I. *Ten lectures on wavelets.* (siam.org, 1992).
 42. Peyré, G. The numerical tours of signal processing. *Comput. Sci. Eng.* (2011).
doi:10.1109/MCSE.2011.71
 43. Paleo, P. PDWT: A GPU implementation of the Wavelet Transform. (2016).
 44. Wang, Z., Bovik, A. C., Sheikh, H. R. & Simoncelli, E. P. Image quality assessment: From error visibility to structural similarity. *IEEE Trans. Image Process.* **13**, 600–612 (2004).
 45. Trauzettel, B., Bulaev, D. V., Loss, D. & Burkard, G. Spin qubits in graphene quantum dots. *Nat. Phys.* **3**, 192–196 (2007).

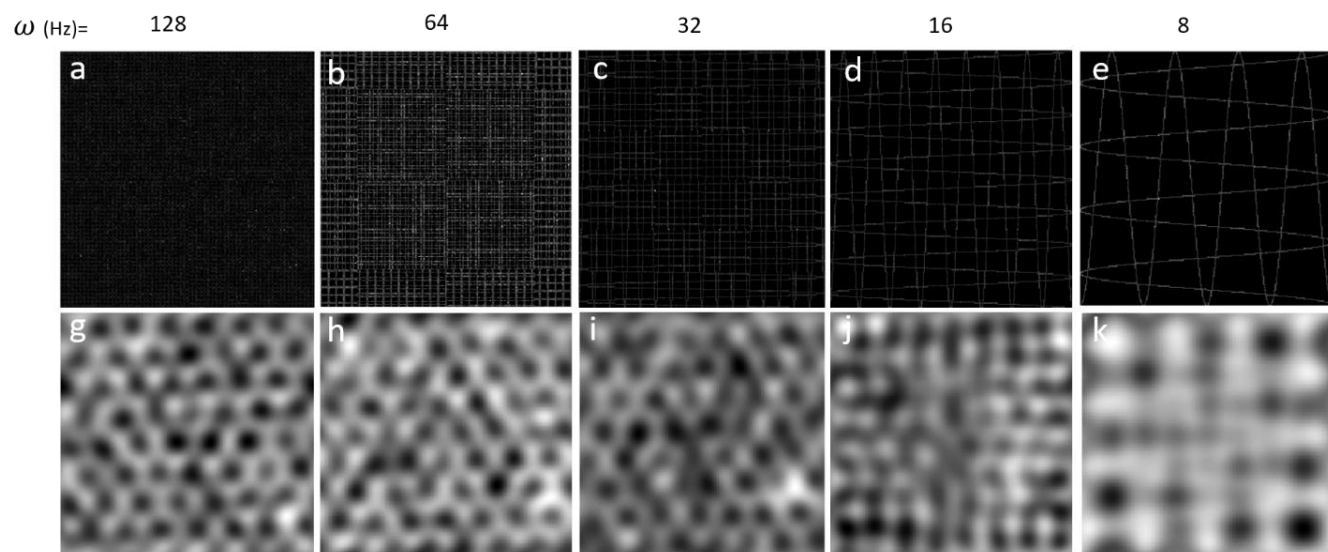
Supplementary Figures:



Supplementary Figure1: Synthetic random scans. (a) Sparse and noisy images. (b) Inpainted results. (c) Numerical evaluations by SSIM.



Supplementary Figure2: Synthetic Lissajous scans. (a-d) Sparse and noisy images. **(e-h)** Corresponding inpainting results.



Supplementary Figure3: Experimental raster scans. (a-d) Sparse and noisy images. **(e-h)** Corresponding inpainting results.